Geotech Geol Eng
https://doi.org/10.1007/s10706-018-0614-8

COMMENTS/DISCUSSIONS AND REPLIES

Numerical Modeling of Shallow Foundation on Liquefiable Soil Under Sinusoidal Loading

Amrendra Kumar · Sunita Kumari

Received: 15 February 2017 / Accepted: 18 June 2018

Abstract In seismic areas, most of the light and heavy structures resting on saturated soil are prone to liquefaction behavior. It occurs in the form of cyclic mobility of soil mass, reduction in bearing capacity, increment in lateral pressure and settlement of structure which must be inspected before constructing any civil engineering structures so that respective precautionary measures can be taken at early stage. The aim of this paper is to model the behavior of shallow foundation on liquefiable soil using Biot's basic theory of porous media. The non-linear behaviors like dilitancy, loading–unloading, hardening and other behaviors of the soil mass are modelled using Pastor–Zienkiewicz Mark III model. Generalized Newmark-beta method is employed for integration in time. A computer code based on finite element method is developed in FORTRAN 90 to simulate a surface footing resting on loose liquefiable soil deposit. The models is subjected to input ground motion of sinusoidal nature to observe the settlement, excess pore pressures, and liquefaction susceptibility of the soil deposits. Some of the key parameters like soil permeability, shear modulus and contact pressure has been also explored on foundation response during numerical study. The results show that settlement of foundations increased with the increase of soil permeability i.e. at higher permeability, maximum settlement in vertical direction and lateral direction are 9.55 cm and 4.20 cm respectively. When shear modulus increases from 8 to 20 MPa, the settlement decreases from 9.55 cm to 2.47 cm in vertical direction and 4.20 cm to 0.98 cm in lateral direction. Excess pore pressures increases with the depth and decreases with the increases in shear modulus.

Keywords Finite element method · Settlement · Footing and excess pore pressures

1 Introduction

Liquefaction is one of the most natural hazardous phenomena, which harms the constructed environment during earthquake. Effect of liquefaction phenomena in the form lateral sliding, settlement, punching shear failure and tilt. Structures situated at shallow depth and lifelines near around the area mostly affected by liquefaction and caused severe destruction and economic losses all over the world. Sometime structures are damaged so badly that it is uneconomical to repair and hence finally demolished.

Earthquake-induced liquefaction is most frequently experiential in loose, saturated, clean sand deposits. This is due to loose sand tends to compress when a

A. Kumar · S. Kumari (✉)
Department of Civil Engineering, National Institute of Technology Patna, Bihar 800005, India
e-mail: amrendraroy2k8@gmail.com

S. Kumari
e-mail: sunitafce@gmail.com

Published online: 22 June 2018

load is applied, disparate to denser sands which tend to dilate during shearing, at least after some strains are enforced. When the fully saturated soil is compressed, the water pressure tends to surge and tries to flow out from the soil to regions having lower pore water pressure. Though, if the loading is large enough and, applied dynamically many times at relatively high frequencies, as in case of an earthquake and other loadings, the undrained condition may result in partial or total effective stress loss called liquefaction. When liquefaction phenomenon occurs, the strength and stiffness of the soil decreases and the ability of a soil deposit to sustain structural load is dramatically reduced. The consequences of liquefaction are seen in terms of permanent deformation, building performance, and ground shaking. These consequences depend on site conditions, earthquake loading characteristics, and structures properties.

Initial time researchers, (Seed and Lee 1966; Seed and Idriss 1971; Castro and Poulos 1977; Seed 1979; Seed et al. 1985; Kramer and Seed 1988) were focused on experimental work to understand the liquefaction phenomenon and cyclic mobility. While the physical phenomenon is well understood, analytical modeling and computer simulation remains a challenge due to complex behavior of soil under seismic loading. Even if liquefaction does not occur, the development of excess pore pressures may lead to excessive soil softening, weakening or to partial loss of stability and even to bearing capacity failures. Rational analysis for the prediction of earthquake generated pore pressures involves a fundamental description of the soil constitutive behavior.

Basically, two-phase porous medium classified as uncoupled and coupled model has been used to study the liquefaction behavior numerically. Numerous investigators including (Finn et al. 1977; Nasser and Shokooh 1979; Liyanapathirana and Poulos 2002) studied the uncoupled investigation of liquefaction in which the response of saturated soil, without considering the effect of soil–water interaction is modeled. The pore water pressure generation and its effect model has been model separately using the results obtained like displacement and volumetric strain. The major dearth in the uncoupled approach is that it is incapable to justify the progressive stiffness degradation caused by pore pressures increment in the soil. The gradual loss of soil stiffness and strength due to build-up of pore water pressures can be model only by coupled approach. In the coupled analysis, all unknowns are computed simultaneously by using a formulation at each time step. Coupled analysis is more convincing representation of the physical phenomena i.e. liquefaction than that provided by uncoupled formulation. (Biot 1955, 1956) developed mixture theory for an elastic porous medium first time for the analysis of liquefaction phenomena. Applications of Biot's theory used for saturated porous media have been used by (Simon et al. 1986) for finite element formulations in wide range of existing problem. (Prevost 1989) integrated the discretized field equations based on the mixture theory and encompassed nonlinear constitutive models for a general analytical procedure. (Oka et al. 1994) pondered the FEM–FDM coupled liquefaction study of a porous soil using elasto-plastic model. (Elgamal et al. 2003) established a computational model for examination of cyclic mobility situations which was based on fully coupled finite element formulations. (Mesgouez et al. 2005) demonstrated use of Biot's theory in transient wave propagation in saturated porous media. (Taiebat et al. 2007) worked on numerical analyses of liquefiable sand using two-surface plasticity critical state model and densification model for bounded soil domain. Some of researchers study the shallow foundation situated on liquefiable soil analysis both experimentally and numerically. (Dashti et al. 2010) conducted Centrifuge test and results shows that building settlement was not related to the thickness of the liquefiable sand layer and that most of this deformation occurs during strong earthquake shaking i.e. depend on intensity of earthquake. (Karamitros et al. 2013) studied the mechanisms of control of seismic liquefaction performance and explained that a naturally or artificially created non-liquefiable soil crust may effectively mitigate the detrimental effects of liquefaction without additional improvement measures. (Dashti and Bray 2013) using the UBCSAND model considering fully-coupled numerical approach simulate in FLAC-2D. Results shows that building settlements is almost same as obtained experimentally for one scaled input motion. (Karimi and Dashti 2016) also performed solid–fluid, fully-coupled 3D nonlinear numerical simulations using the PDMY02 soil model. (Mehrzad et al. 2016) analyzed the result as soil permeability (k) increases settlement of foundations increases. Excess pore water pressure and settlement mechanisms were captured by the soil

model. (Banerjee et al. 2017) studied the liquefaction behavior of Kasai River Sand. Results shows the amplification of the peak ground acceleration for the saturated sand is 1.08 and 1.32 times higher than that for the dry sand from theoretical and experimental results.

In the present study, for simulation of behavior of shallow foundation on liquefiable soil domain finite element analysis based on coupled algorithm is considered for developing appropriate numerical models. The generalized Biot's theory has been used for a deforming saturated porous medium to develop the governing equilibrium and continuity equations. The soil domain is discretized into isoperimetric elements having 8 node for displacement and 4 node for pore pressure node. The primary unknowns are taken as displacements and the fluid pressure in the framing of finite element analysis for the numerical modeling. Kelvin elements are attached to transmitting boundary to absorb the wave energy generated due to boundary condition. It also prevents back propagation of wave into the soil domain. Newmark-beta integration scheme is used to solve the continuity equations and dynamic equilibrium equation with in time domain. The Pastor–Zienkiewicz Mark III model (Pastor and Zienkiewicz 1986) has been used to explain the inelastic behavior of soils under isotropic cyclic loadings. The effect of the material nonlinearity of the soil grain on liquefaction response is investigated by conducting a parametric study for key parameters like soil permeability, shear modulus and surcharge.

2 General Formulation

For a fully coupled formulation, equilibrium or momentum balance equation for the soil–fluid mixture and mass balance equation for the whole system of soil mass including fluid must be satisfied. The unknowns in this formulation are displacement of solid phase (U_s), displacement of fluid phase relative to the solid phase (U_{rf}), and pressure of fluid phase (P). For dynamic problems high-frequency oscillations is insignificant. (Zienkiewicz et al. 1999) studied the problems under earthquake loading, the relative velocity of fluid phase has little influence or insignificant on the system and can be eliminated. Therefore, the equations for mass balance and fluid momentum balance can be group together and as a result the governing equations are reduced to two. The primary variables in this form of equations are fluid pressure and soil solid displacement. Thus, this form is called U_s–P or for simplicity U–P formulation. Hence, displacements and pore pressures are calculated at the same time and interactively at each time step.

Finite element method for spatial discretization, U–P formulation is as follows:

$$[M]\left\{\ddot{U}_e\right\} + [K]\left\{U_e\right\} - [Q]\left\{P_e\right\} = \left\{f_U\right\} \tag{1}$$

$$[G]\left\{\ddot{U}_e\right\} + [Q]^T\left\{\dot{U}_e\right\} + [S]\left\{\dot{U}_e\right\} + [H]\left\{P_e\right\} = \left\{f_P\right\} \tag{2}$$

where $[M]$ is the mass matrix, $[K]$ is the stiffness Matrix, $[Q]$ is the coupling Matrix, $[f_U]$ is the force matrix, $[G]$ is the dynamic coupling matrix, $[H]$ is the permeability Matrix, $[S]$ is the compressibility Matrix, $[f_P]$ is the force matrix for fluid phase of an element.

From Eqs. (1) and (2) the numerical solutions of can be accomplished by integrating the equations in each time domain, which can be extrapolated to the next time instance (t_{n+1}), (Katona and Zienkiewicz 1985) using known previous initial conditions by employing generalized Newmark method. The primary unknown assumed incremental in the form of displacements ΔU and pore pressure ΔP and the final equations is achieved as follows:

$$\begin{aligned}&(L_1[M] + [K])\{\Delta U_i\} - [Q]\{\Delta P_i\}\\ &\quad = \Delta f_U + [M]\left(L_2\dot{U}_{i-1} + L_3\ddot{U}_{i-1}\right)\end{aligned} \tag{3}$$

$$\begin{aligned}&\left(L_1[G] + L_4[Q]^T\right)\{\Delta U_i\} - (L_2[S] + [H])\{\Delta P_i\}\\ &\quad = \Delta f_P + [G]\left(L_2\dot{U}_{i-1} + L_3\ddot{U}_{i-1}\right)\\ &\qquad + [Q]^T\left(L_5\dot{U}_{i-1} + L_6\ddot{U}_{i-1}\right)\end{aligned} \tag{4}$$

$$L_1 = {}^1\!/_{(\beta\Delta t^2)};\ L_2 = {}^1\!/_{\beta\Delta t};\ L_3 = {}^{0.5}\!/_{\beta}$$
$$L_4 = {}^{\alpha}\!/_{(\beta\Delta t)};\ L_5 = {}^{\alpha}\!/_{\beta};\ L_6 = {}^{0.5}\!/_{\beta} - 1$$

In which, α and β are generalized Newmark method parameters and Δt is the time step. The vectors $\dot{U}_t$,$\ddot{U}_t$ and $\dot{P}_t$ can be evaluated explicitly from the information available at time t_n.

The surface footing is assumed to be at top surface resting on center of domain. The load vector is distributed as follows:

$$\{Q\}_e = \int_{-1}^{1} Q_z \begin{Bmatrix} \frac{1}{2}(\zeta + \zeta^2) \\ (1 - \zeta^2) \\ \frac{1}{2}(-\zeta + \zeta^2) \end{Bmatrix} d\zeta \tag{5}$$

where Q is applied surcharge per unit length. ζ is the Cartesian coordinate in x direction.

In dynamic equation, viscous damping is incorporated for solid phase in the form of $[R_m]\{\dot{U}\}$ where R_m is called the Rayleigh damping (Patil et al. 2013).

$$[R_m] = \delta_1[M] + \delta_2[K] \tag{6}$$

The coefficients δ_1 and δ_1 can be obtained by selecting a damping ratio ζ_n and a certain frequency ω_n such that

$$\zeta_n = \frac{\delta_1}{2\omega_i} + \frac{\delta_2 \omega_i}{2} \tag{7}$$

3 Soil Constitutive Model

For describing the basic equation of the generalized plasticity model Pastor et al. (1990) model for sands has been used. In this model both volumetric and deviatoric plastic strains are included in the hardening and dilitancy parameter of the bounding surface. In addition, plastic volumetric and deviatoric strains are introduced during unloading.

The elastoplastic behavior can be defined by a relation between stress (σ) and strain (ε) increments as:

$$d\sigma = E^{ep} : d\varepsilon \tag{8}$$

In which, E^{ep} is elastoplastic constitutive matrix depends on the state and history of stress–strain, and the direction of strain increment $d\varepsilon$. E^{ep} is defined by following relation [8].

$$E^{ep} = E^e - \frac{E^e n_{gL/U} n^T E^e}{H_{L/U} + n^T E^e n_{gL/U}} \tag{9.1}$$

In which, E^{ep} signifies the elastic constitutive matrix, n is vector of normal in loading direction, $n_{gL/U}$ is flow direction vector during loading or unloading condition, and $H_{L/U}$ is defined as plastic modulus under loading and unloading condition respectively.

The stress increment direction is distinguished as loading or unloading from unit normal $\boldsymbol{n}$ as defined by the following expressions:

$$d\sigma = E^L \, d\varepsilon \qquad if \; n^T d\sigma > 0 \text{ (Loading)} \tag{9.2}$$

$$d\sigma = E^U \, d\varepsilon \qquad if \; n^T d\sigma < 0 \text{ (Unloading)} \tag{9.3}$$

Neutral loading is defined by $n^{\mathrm{T}} d\sigma = 0$ when both loading and unloading moduli are identical and the behavior is locally elastic. The different parameters of Pastor–Zienkiewicz Mark III Model have been taken from (Kumari et al. 2016).

The isotropic hypo-elasticity behavior is assumed in the present model and is defined as:

$$\dot{\varepsilon}_q^e = \frac{\dot{s}}{2G}; \; \dot{\varepsilon}_V^e = \frac{\dot{p}}{K} \tag{10}$$

where $\dot{\varepsilon}_q^e$ and $\dot{\varepsilon}_V^e$ are the elastic components of the deviatoric and the volumetric strain increments respectively. $\dot{s}$ and $\dot{p}$ are the deviatoric and the mean effective stress increment tensor. The elastic shear modulus (G) and elastic bulk modulus (K) are adopted from (Pastor et al. 1990).

$$K = K_0 \frac{p}{p_{at}} \quad and \quad G = G_0 \frac{p}{p_{at}} \tag{11}$$

where p_{at} is the atmospheric pressure used as a reference pressure, for which $K = K_0$ and $G = G_0$.

4 Comparison of Numerical and Experimental Results

For soil liquefaction behavior and modeling, the centrifuge modeling has been considered among the best experimental methods. The stress conditions generated during the said phenomena can be closely simulated to the full-scale prototype model. Hence, the correctness and accuracy of the proposed finite element based solution algorithm are authenticated by comparing the numerical results obtained with the centrifuge model test results, conducted at the RPI centrifuge facility. The soil used in all models is a fine, uniform Nevada sand with $D_{50} = 0.13$ mm. The permeability of the sand calculated by standard ASTM code in the laboratory at $1\,g$ is $k = 0.0021$ cm/s. The input motion frequency was so selected to reduce the potential for amplification in the model. It was subjected to an acceleration

field of 80 g. In the present study, the saturated loose soil domain of size 24 m × 15 m have been used and Surcharge of 0.1 t/m^2 as shallow foundation was applied at the surface, and the maximum initial effective stress at the base was 150 kPa. A cross section of centrifuge model used by Liu and Dobry (1997) showing the locations of the pore pressure transducers and accelerometers are shown in Fig. 1 and material properties are reported in Table 1.

The measured excess pore pressure time histories at depths of 2, 4, and 8 m are validated with the developed model, result as shown in Figs. 2, 3, and 4. It is seen that at a depth of 2 m, the maximum EPP obtained from centrifuge test is 29.3 kPa whereas this value is 29.8 kPa in case of coupled finite element study. These two values are very close to each other. Similar trend is also seen at 4 and 8 m depth. Figure 5 shows the comparison of settlement obtained in between centrifuge test and developed model. The present study shows the maximum settlement of 5.98 cm and 6 cm are observed at top surface of soil domain in case of numerical modeling and centrifuge study respectively.

The time to reach 100% pore pressure rise increases with depth, indicating that liquefaction occurs first near the surface and progress in vertically downward vertical direction. At depth of 8 m, the maximum computed EPP (76 kPa) is slightly higher than the experimental value (67.32 kPa). The cause for this discrepancy may be due to use of constant permeability coefficient, which does not similar to the real conditions, when liquefaction has initiated. Results are showing fairly good agreement with result presented by Liu and Dobry (1997) with little deviation. Hence, the comparison demonstrates that the present model can roughly simulate the real condition behavior of liquefaction phenomena.

Table 1 Parameters selected from RPI Centrifuge model tests [Liu and Dobry (1997)]

Parameter	Value
Centrifuge acceleration (g)	80
Fluid viscosity	60
Prototype soil depth (m)	15.0
Surcharge load (kPa)	0.1 t/m^2
Relative density, D_r (%)	50
Permeability, k (m/s)	2.1×10^{-6}

5 Overview of Numerical Simulation

A saturated soil domain consists of loose sand layer having depth 15 m and width 24 m is considered for the numerical simulation in two-dimensional plane-strain conditions. The top 10 m soil if sandy in nature whereas the underlying soil strata 5 m are gravel in nature. The mesh consideration for finite element discretization has 180 elements as shown in Fig. 6. The FEM code has been written in FORTRAN 90. The variation of excess pore pressure and displacement with time has been used for the response analysis. A static analysis is performed before applying cyclic load.

5.1 Static Analysis

A static analysis is performed to apply the gravitational forces due to self-weight of the soil and

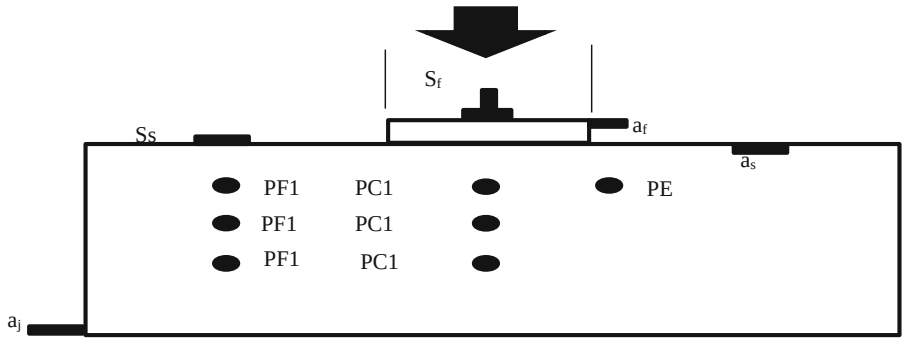

Fig. 1 Cross-section of the centrifuge model and instrumentation layout [modified after Liu and Dobry (1997)]

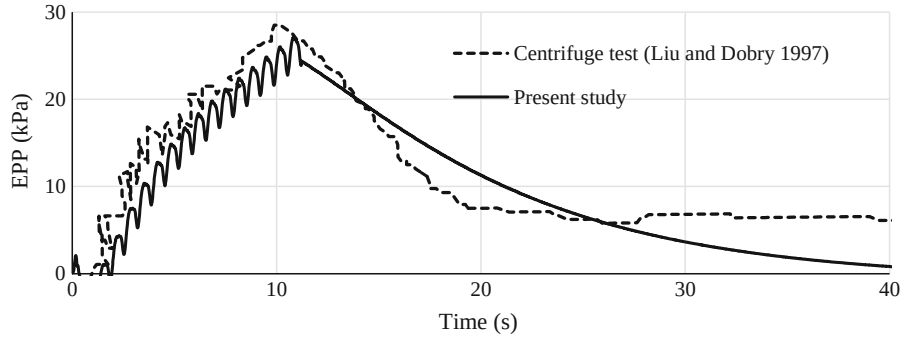

Fig. 2 Excess pore pressure verses time at 2 m depth

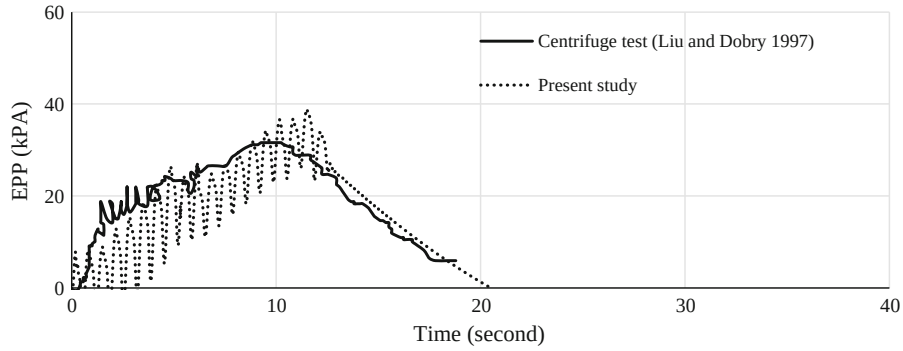

Fig. 3 Excess pore pressure verses time at 4 m depth

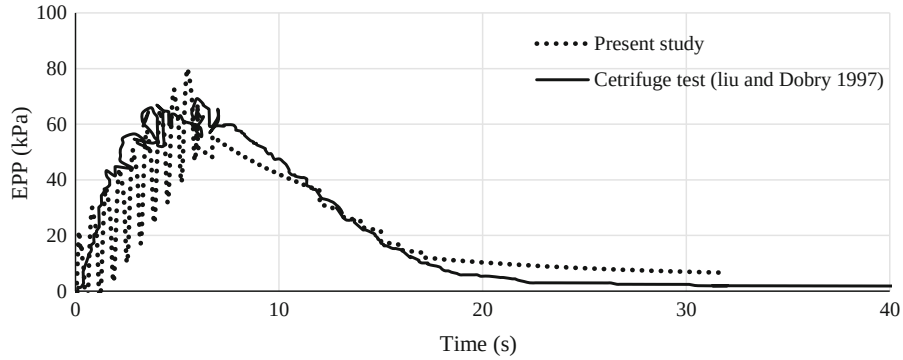

Fig. 4 Excess pore pressure verses time at 8 m depth

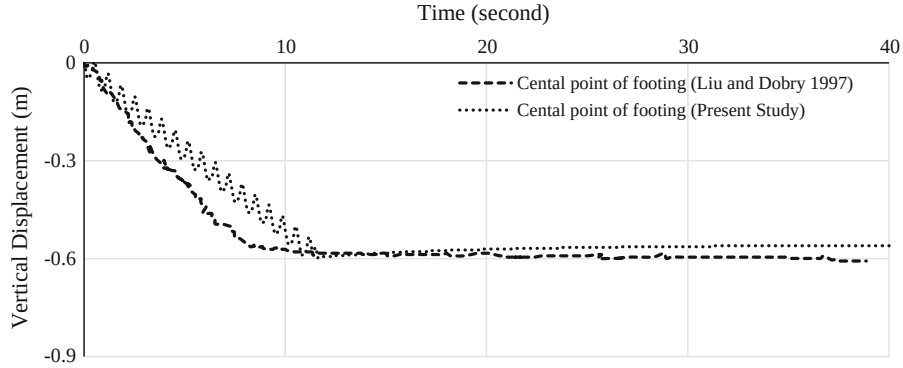

Fig. 5 Variation of settlement center of foundation at surface

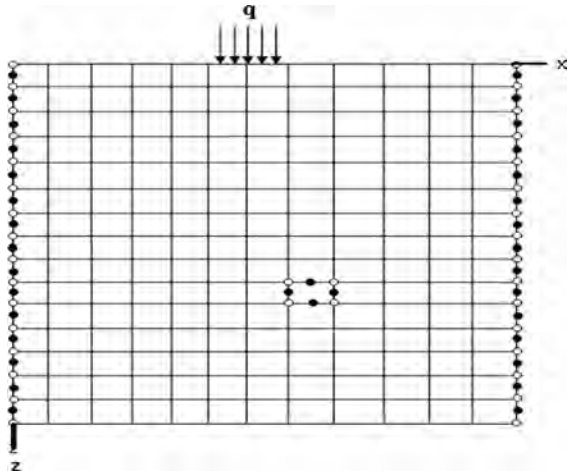

Fig. 6 Soil domain having 8–4 node mixed element

foundation before cyclic excitation. The resulting initial stress is evaluated throughout the considered domain due to hydrostatic pressures of fluid and used as initial conditions for the subsequent dynamic analysis. The coupled equations of consolidation analysis have been considered for the static analysis are given as:

$$[K]\{U_e\} - [Q]\{P_e\} = \{f_U\} \tag{12}$$

$$[Q]^T\{\dot{U}_e\} + [H]\{P_e\} = \{f_P\} \tag{13}$$

5.2 Dynamic Analysis

The equilibrium condition is attained after evaluating initial stress condition. Then, a nonlinear analysis is performed for the harmonic load with the supplied horizontal and vertical cyclic acceleration $a = a_o \sin\omega t$. The dynamic analyses are performed using a Generalized Newmark scheme with nonlinear iterations by taking initial linear elastic tangential global matrix. The numerical integration parameters of the generalized Newmark's method are selected as $a = 0.60$ and $b = 0.3025$ for the dynamic analysis. The material parameters used here are described in Table 1.

The time step used is usually governed by time of cyclic loading and frequency of the input motion. Void ratio, coefficient of permeability and other properties were kept constant during the analysis. The elastic shear modulus (G) and elastic bulk modulus (K) are changing at each time step in accordance with Eq. (11) which will counter the effect of change in void ratio during cyclic loading. Rayleigh damping of 5% is applied at the prevailing frequency motion enhance the energy dissipation characteristic of the constitutive model. For 64 cycles of the loading motion, the numerical simulation has been performed. The amplitude and frequency of the cyclic loading were $a_0 = 0.2$ g and 1.5 Hz respectively. A surface footing of intensity 0.1 t/m^2 is assumed to be resting at top surface of the central position element of saturated sand layer.

6 Result and Discussion

The liquefaction behavior of saturated sand has been numerically simulated using the fully coupled formulation. The input parameters i.e. frequency 1 Hz, surface loading 0.1 t/m^2, permeability of 1.68×10^{-4} m/s and shear modulus of 10 MPa have used for present analysis.

Figures 7, 8 displays the computed horizontal and vertical displacement below the footing at left, center and right side. The maximum values of horizontal settlement of 4.32 cm and vertical settlement of 9.4 cm are predicted at the top of soil layer below the right of footing. The value obtained at right side is higher than the left side which may be due to amplification of the seismic wave. It has been also observed that most of the settlements occur during the shaking period that is before 15 cycles. A decreasing or constant trend is observed for settlement after completion of cyclic load. Generally, the horizontal settlement is less than vertical settlement at different depths.

Figure 9 displays the computed excess pore pressure at different depth. Pore pressure began to increase once input cyclic load imparted to the soil domain. The computed pore pressure time histories indicate that soil at Z/B is 1.0, 1.5, 2.0 and 2.5 is not liquefied because excess pore pressure (EPP) is less than initial vertical stress except at Z/B at 0, and 0.5. At Z/B equal to 0, and 0.5 i.e. at shallow depth, liquefaction occurs, the generation of pore water pressure is more than the effective stress (Mehrzad et al. 2016). This behavior of high EPP at shallow depth below the foundation is observed due to the generation of horizontal and vertical hydraulic gradients. These gradients are generated due to pore water pressure difference

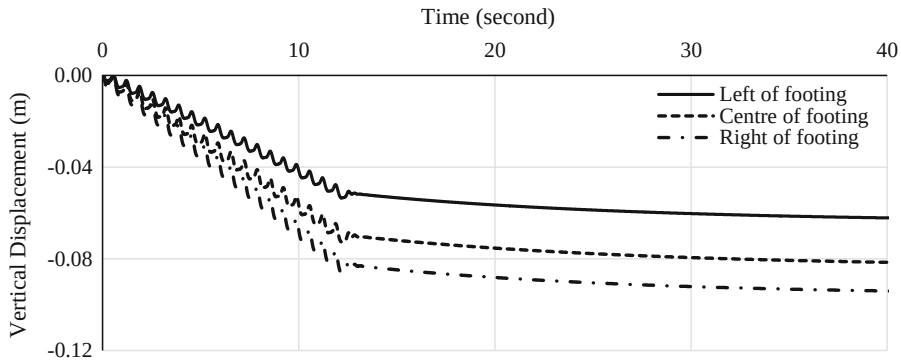

Fig. 7 Computed vertical displacement with respect to time

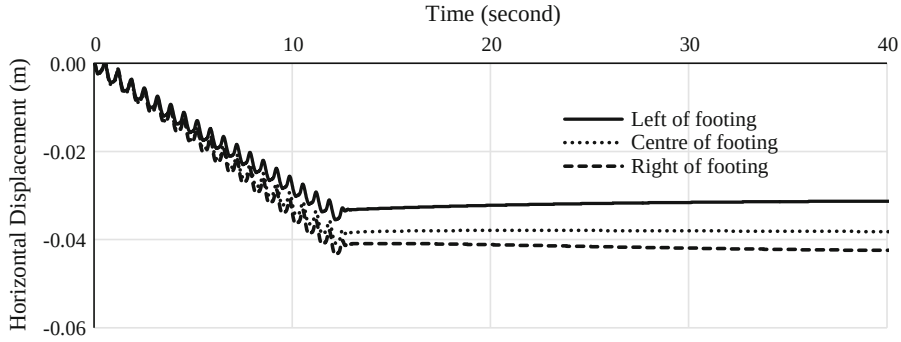

Fig. 8 Computed horizontal displacement with respect to time at below the footing

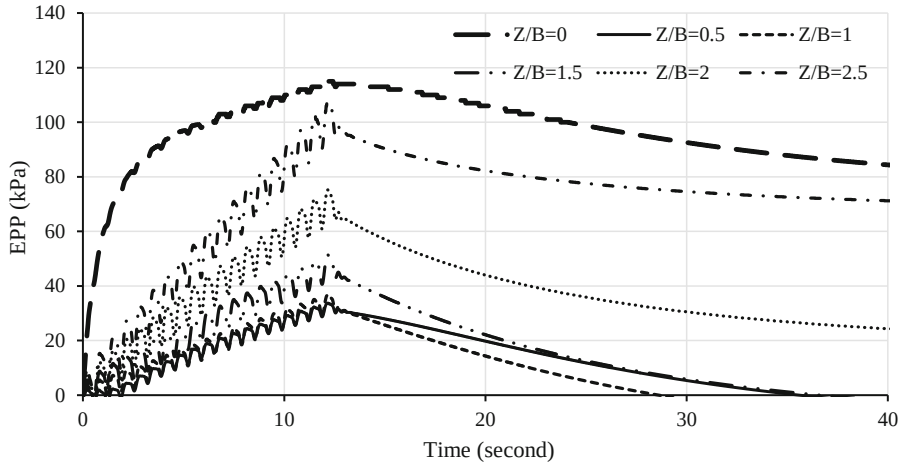

Fig. 9 Computed EPP at center of footing with respect to time

between soil beneath the foundation and free field. EPP equalized in each level which results in disappearance of lateral water flow and horizontal hydraulic gradients. Then, EPP took a constant value for relatively long time; soil profile started to reconsolidate from the bottom of container and resultant upward seepage due to reconsolidation of deeper layers, prevented EPP reduction in shallower layers. Finally, EPP completely dissipated in all the layers. It also seems that dissipation of excess pore pressure is slow at shallow depth after completion of cyclic loading. At Z/B = 3.0 of soil domain, rise in excess pore pressure is zero due to existence gravel layer of higher permeability at bottom, hence no liquefaction phenomena observed.

The stress paths depicted in Figs. 10 and 11 show the typical mechanism of cyclic motion reduction in effective stress due to increases in pore pressure,

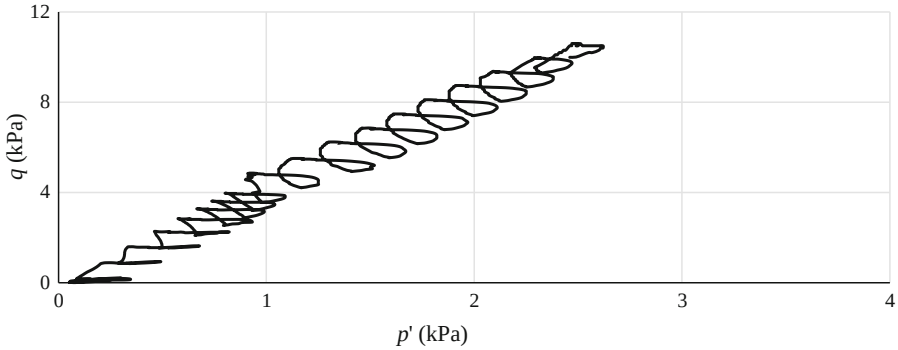

Fig. 10 Computed effective stress path at 1.5 m

captured using the Pastor–Zienkiewicz Mark III model. It is observed that maximum stress ratio q/p (effective stress/pore water pressure) is 3.98 at the depth of 1.5 m (Fig. 10) and 0.95 at the depth of 11.5 m (Fig. 11) respectively. This value decreases as depth increases mainly due to effect of effective stress. Similar variation in q with time at different depths is presented in Fig. 12. Maximum values of q are 10.4, 8.8, 2.7, 2.1, 1.57, and 0.22 (kPa) at depths 1.5, 3.5, 5.5, 7.5, 9.5 and 11.5 m, respectively. These maximum values of q are showing almost linearly increasing trend with depth.

Figures 13 and 14 show that the variation of normalized vertical and horizontal acceleration with respect to the time at different normalized depth (Z/B). It has been detected that the highest value of normalized acceleration is found to be about 0.16 at $Z/B = 0.5$, resulting greater settlement. Relatively less value of accelerations is seen at $Z/B = 2.0$ depth, equivalent to lesser excess pore pressure. It noticeably indications of the amplification in ground acceleration from base to the top surface. Acceleration is quantified in both directions after the end of 13 cycle of loading is negligible, at which liquefaction is occurring at some sacks of soil domain. Results indicate that amplification of cyclic input motion from base to the top surface presenting maximum value at $Z/B = 0.5$. (Anbazhagan et al. 2006) indicated that the amplification of cyclic input motion is one of the causes of liquefaction in shallow depth of soil.

6.1 Effect of Shear Modulus

The effect of shear modulus is also studied for shallow foundation on liquefiable soil at an acceleration of 0.2 g m/s^2. The shear modulus (G) has been varied as 8, 12, 16, and 20 MPa respectively, while keeping other parameters constant. The relative density of the sand is taken as 54%. The study is carried out at two values of permeability e.g. 1.68×10^{-4} and 2.1×10^{-6} m/s respectively. The variation of displacement with respect time at different shear modulus is shown in Figs. 15 and 16 respectively.

A decreasing trend is noticed for both type of displacement in vertical and horizontal direction as the value of shear modulus is increased. It is also observed

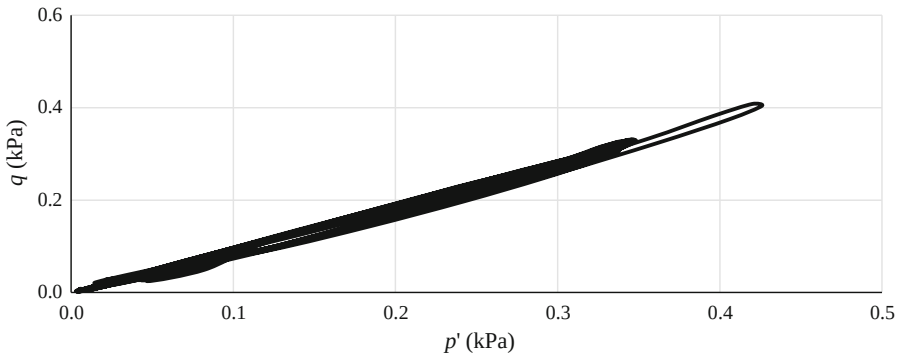

Fig. 11 Computed effective stress path at depths 11.5 m

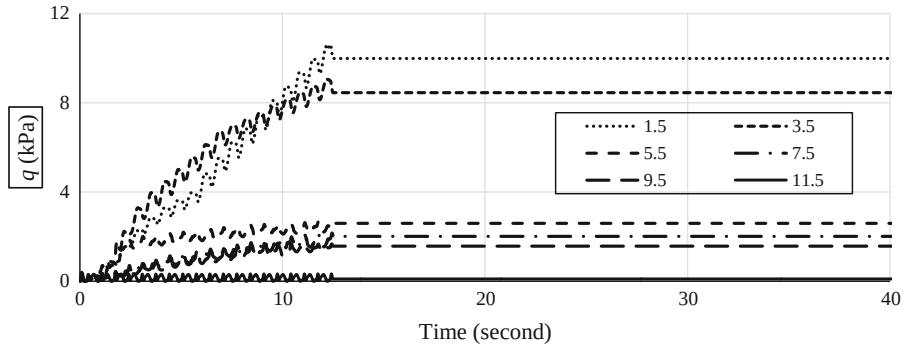

Fig. 12 Computed q (kPa) v/s time at different depth (m)

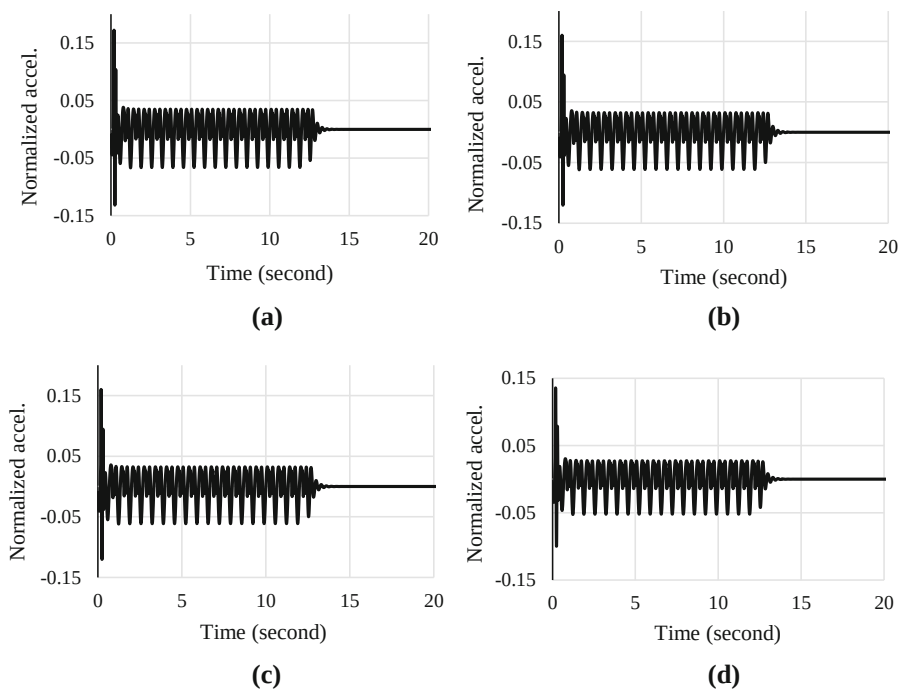

Fig. 13 Normalized vertical acceleration v/s time. **a** $Z/B = 0.5$, **b** $Z/B = 1.0$, **c** $Z/B = 1.5$, **d** $Z/B = 2.0$

that the maximum horizontal settlement (4.02 cm) and the maximum vertical settlement (9.55 cm) occur at 8 MPa respectively. This behavior is occurring due to increases in stiffness of the soil. The vertical settlement is higher than that of horizontal settlement. The effect of permeability is also studied. A decreasing trend of displacement is seen with decrease in permeability due to increase in pore pressure. In vertical displacement about 16% reduction observed with reduction of permeability from 1.68×10^{-4} to 2.1×10^{-6} m/s, whereas the horizontal displacement variation is only 2–4% which is not significant.

The effect of shear modulus on peak value of effective pore pressure at different depth is shown in Fig. 17. It is seen that at 2 m depth, EPP variation with respect to shear modulus is negligible because of development of high pore pressure. At this depth, liquefaction is occurring at frequency 1.5 Hz for a particular value of cyclic loading. It is also seen that liquefaction occurs at shear modulus of 8, 12, 16 and 20 MPa for this particular value of frequency. Hence, it may be concluded that for a particular value of dynamic loading and frequency, liquefaction may also occur for soil strata having higher shear modulus.

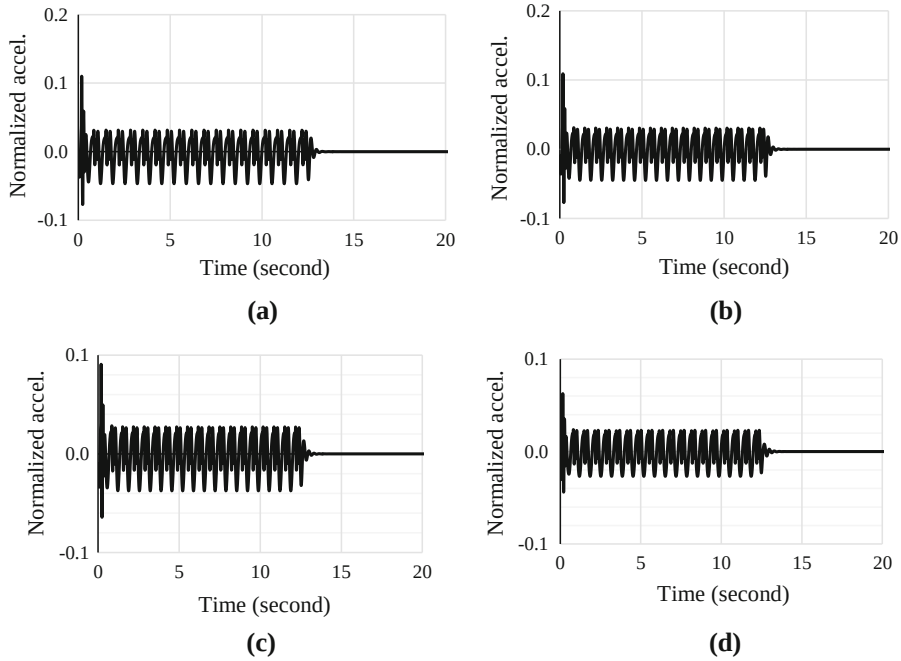

Fig. 14 Normalized horizontal acceleration v/s time. **a** $/B = 0.5$, **b**)$Z/B = 1.0$, **c** $Z/B = 1.5$, **d** $Z/B = 2.0$

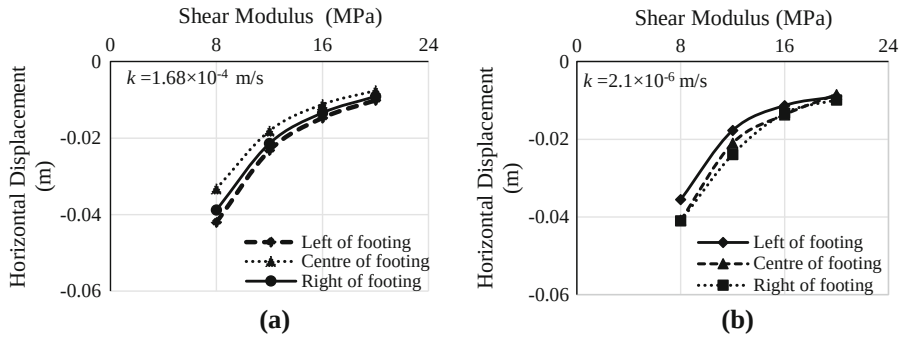

Fig. 15 Variation of horizontal displacement v/s shear modulus **a** $k = 1.68 \times 10^{-4}$ m/s **b** $k = 2.1 \times 10^{-6}$ m/s

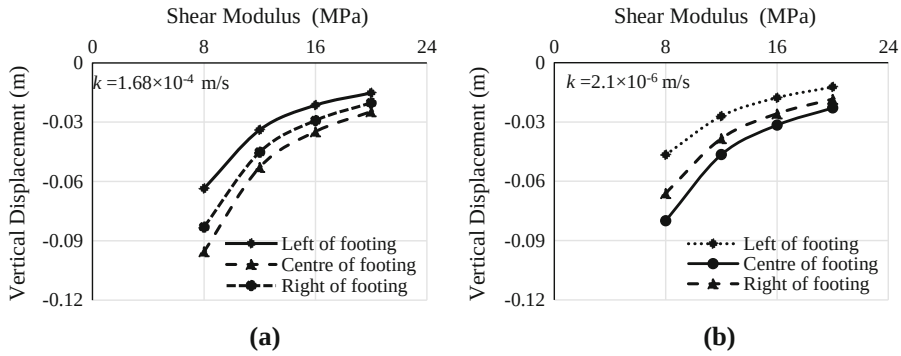

Fig. 16 Vertical displacement v/s shear modulus **a** $k = 1.68 \times 10^{-4}$ m/s **b** $k = 2.1 \times 10^{-6}$ m/s

Figure 17 shows that as the value of permeability decreases within range of loose sand, increase in excess pore pressure occurs (Mehrzad et al. 2016).

Figure 18 shows the variation of effective pore pressure with time at different shear modulus and permeability. The variation of results shows that at surface and shallow depth the chance of liquefaction is

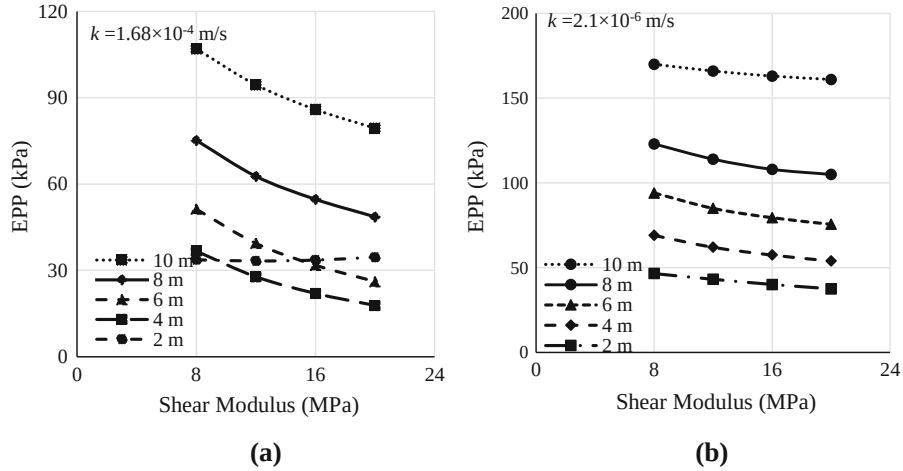

Fig. 17 Variation of effective pore pressure (EPP) at different permeability and Shear Modulus (G)

more because of higher value of develop pore pressure. But as the Z/B ratio increase the chance of liquefaction reduces due to higher value of effective stress by soil mass and surcharge. Permeability also play a crucial role for development of pore pressure. At lower value of permeability, there is a sharp rise in excess pore pressure and thus liquefaction occurs. At $k = 2.1 \times 10^{-6}$ m/s, liquefaction is occurring at almost every depth.

Table 2 shows the variation of displacement at different location below footing. As the value of shear modulus increases the value of displacement decreases. The maximum displacement reduces about 55% below the footing when double the value of shear modulus i.e. from 8 to 16 MPa. The effect of permeability also tabulated, the variation of horizontal displacement is not much more but the vertical displacement the reduction in about 16% when the permeability is reduces.

Table 3 shows the variation of effective pore pressure with permeability and shear modulus. At higher permeability the liquefaction will occurs near the surface about 2 m depth. But at lower permeability liquefaction will occurs at every depth up to 10 m. After 10 m no liquefaction will observed due to presence of gravel layer. It is also observed that soil with high permeability, excess pore water pressure decrease dramatically after shaking ceased; therefore, the amount of foundation settlement was very small during this period.

6.2 Effect of Surcharge

Foundations are rigid surface footing resting on the liquefiable ground have been used to investigate the liquefaction effect. Each light and heavy foundation having surcharge of 0.1 and 0.15 t/m^2 respectively have been analyzed individually to study the effect of surcharge. Surcharge consider as total load including foundation load also. Table 4 shows the vertical and horizontal displacement of footing under the considered load. It is found that at higher value of surcharge, there is a sharp increase in vertical and horizontal displacement as compare to the lower value of surcharge. At a loading of 0.1 t/m^2, the maximum vertical displacement at center is 8.31 cm whereas at 0.15 t/m^2, maximum displacement is 12 cm. Horizontal displacement also increase from 4.08 to 6.1 cm. Most of heavy foundations' settlement occurred during shaking due to partial drainage and shear stress applied by heavy foundation.

Pore pressure ratio is also evaluated at different depth ratio (Z/B) and shear modulus (G) respectively. Pore pressure ratio r_u is defined as the ratio of excess pore pressure, and initial vertical effective stress. Table 5 represents the respective results. At Z/B = 1.0, no liquefaction is visible for light weight footing whereas for heavy weight footing liquefaction is seen at lower shear modulus. Also, a pore pressure ratio at greater than one at shallow depth at different value of shear modulus. So, there is a clear indication of liquefaction just below footing and hence mitigation of the problem should be suggested before

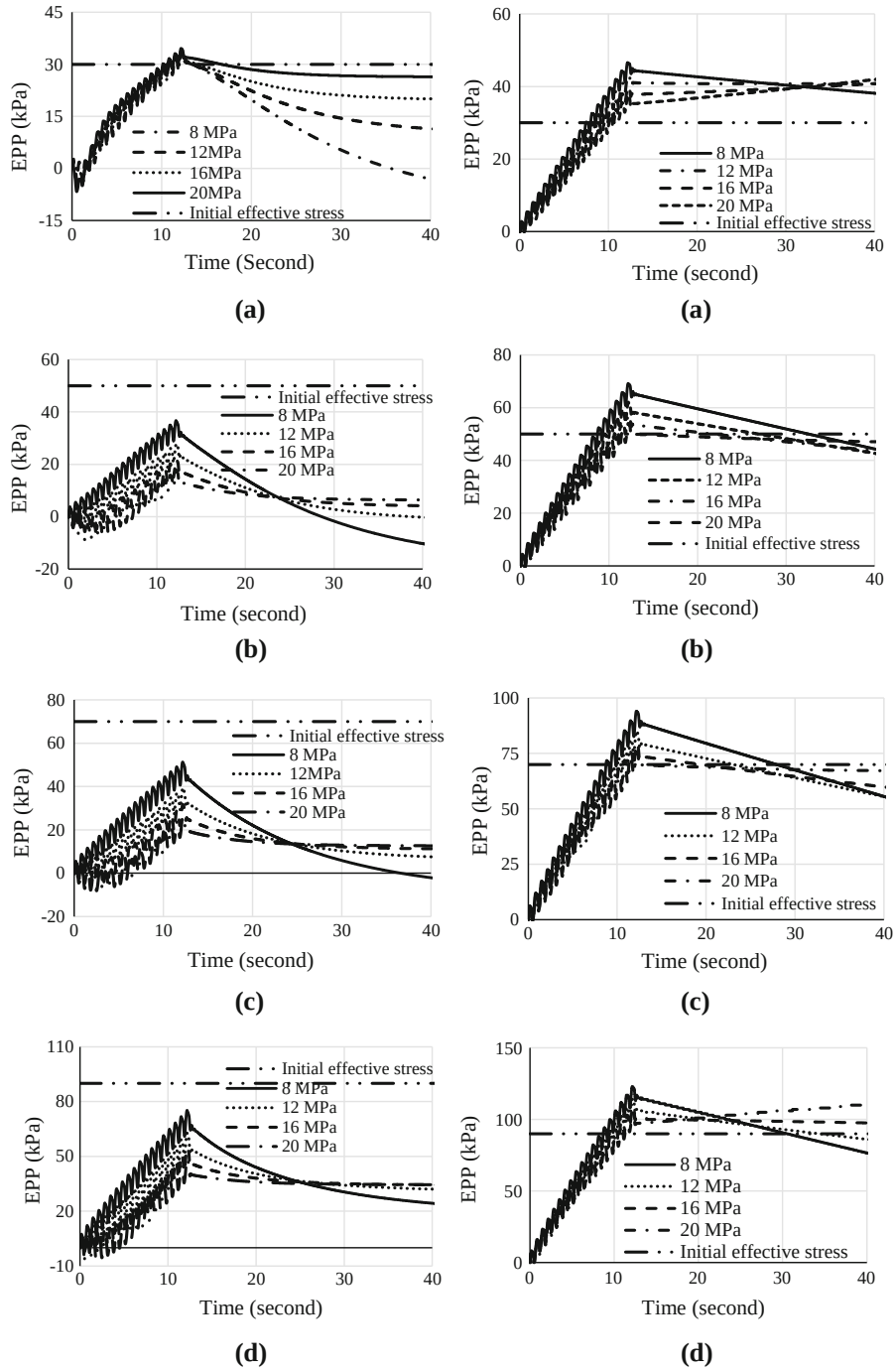

Fig. 18 Variation in EPP with time for different shear modulus and at $k = 1.68 \times 10^{-4}$ m/s and 2.1×10^{-6} m/s **a** $Z/B = 0.5$, **b** $Z/B = 1.0$, **c** $Z/B = 1.5$, **d** $Z/B = 2.0$

constructing any structure. After analyzing different r_u value that chance of liquefactions is reduced at higher value of shear modulus at some of intermediate points.

7 Conclusions

The numerical analysis of shallow foundation in cyclic loading conditions has provided valuable understandings regarding the evaluation of liquefaction-induced foundation settlement and effect of pore water

Table 2 Variation of displacement at different location below footing

Permeability	Displacement (cm)						
		Z-direction			X-direction		
	G (Pa)	Left	Centre	Right	Left	Centre	Right
$k = 1.68 \times 10^{-4}$	8	6.36	8.31	9.55	3.55	4.08	4.2
	12	3.39	4.52	5.28	1.77	2.1	2.39
	16	2.14	2.92	3.48	1.13	1.37	1.33
	20	1.52	2.03	2.47	0.898	0.847	0.985
$k = 2.1 \times 10^{-6}$	8	4.66	6.61	8.0	3.32	3.88	4.1
	12	2.7	3.84	4.65	1.81	2.14	2.32
	16	1.77	2.58	3.16	1.12	1.34	1.47
	20	1.23	1.84	2.29	0.76	0.911	1.01

Table 3 Variation of EPP at different *Z/B* ratio below footing

Frequency (Hz) = 1.5	Maximum EPP at different depth (kPa)					
	G (MPa)	*Z/B* = 0.5	*Z/B* = 1.0	*Z/B* = 1.5	*Z/B* = 2.0	*Z/B* = 2.5
$k = 1.68 \times 10^{-4}$	8	33.7	36.7	51.3	75.2	107
	12	33.3	27.8	39.4	62.7	94.5
	16	33.6	22	31.8	54.7	85.9
	20	34.6	17.8	26.1	48.6	79.4
$k = 2.1 \times 10^{-6}$	8	46.6	69.1	94.1	123	170
	12	43.2	62.1	85	114	166
	16	40.1	57.5	79.5	108	163
	20	37.5	54	75.6	105	161

Table 4 Horizontal and vertical displacement below the footing

G (MPa)	Horizontal displacement		Vertical displacement	
	0.1 (t/m^2)	0.15 (t/m^2)	0.1 (t/m^2)	0.15 (t/m^2)
8	4.08	6.1	8.31	12
12	2.10	3.4	4.52	6.58
16	1.37	2.2	2.92	4.28
20	0.85	1.5	2.03	3.09

pressure which is primarily controlled by shear modulus, permeability and intensity of earthquake. A maximum vertical settlement of 9.5 cm and horizontal displacement of 4.2 cm are observed at right of the footing surface of the soil domain. At higher value of shear modulus ($G = 20$ MPa), liquefaction does not occur within the soil domain except at $Z/B = 0$ and 0.5. As the shear modulus is reduced, liquefaction of soil is observed because of higher displacement and excess pore pressure. It is also observed that maximum stress

Table 5 Pore pressure ratio (r_u) at different surcharge

G (MPa)	*Z/B* = 0.5		*Z/B* = 1.0		*Z/B* = 1.5		*Z/B* = 2.0		*Z/B* = 2.5	
	0.1 (t/m^2)	0.15 (t/m^2)	0.1 (t/m^2)	0.15 (t/m^2)	0.1 (t/m^2)	0.15 (t/m^2)	0.1 (t/m^2)	0.15 (t/m^2)	0.1 (t/m^2)	0.15 (t/m^2)
8	1.12	1.45	0.73	1.07	0.73	1.07	0.84	1.19	0.97	1.37
12	1.11	1.41	0.56	0.86	0.56	0.87	0.70	1.03	0.86	1.23
16	1.12	1.48	0.44	0.84	0.45	0.86	0.61	1.05	0.78	1.24
20	1.15	1.48	0.36	0.74	0.37	0.77	0.54	0.97	0.72	1.17

ratio q/p is 0.98 at the depth ratio of $Z/B = 0.25$, which declines with depth mainly due to effect of initial effective stress. This results in development of higher excess pore pressure at shallow depth. Permeability also plays important role, if the permeability is low generation of pore water pressure is high so chance of liquefaction increases.

The mathematical gain of this numerical model is that the estimation of excess pore pressure and displacement can be done simultaneously without using any empirical relationship at any point of time. So, it does not require experimental identification for the prominent effecting parameter. This model is also validated with centrifuge experimental results and shows good agreement. Hence, the developed numerical formulation can be easily suggested to practicing engineers to for predicting the dynamic performance of geotechnical site and key parameters.

References

Anbazhagan P, Sitharam TG, Divya C (2006) Site amplification and liquefaction studies for Banglore City, Indian Geotechnical Conference, 14–16 Dec., Chennai, India

Banerjee R, Konai S, Sengupta A, Deb K (2017) Shake table tests and numerical modeling of liquefaction of Kasai River Sand. DOI, Geotech Geol Eng. https://doi.org/10.1007/s10706-017-0178-z

Biot MA (1955) Theory of elasticity and consolidation for a porous anisotropic solid. J Appl Phys 26:182–185

Biot MA (1956) Theory of propagation of elastic waves in a fluid saturated porous solid. J Acoust Soc Am 28(2):168–178

Castro G, Poulos SJ (1977) Factors affecting liquefaction and cyclic mobility. J Geotech Eng ASCE 103(GT6):501–516

Dashti S, Bray JD (2013) Numerical simulation of building response on liquefiable sand. J Geotech Geoenviron Eng 139(8):1235–1249

Dashti S, Bray JD, Pestana JM, Riemer MR, Wilson D (2010) Mechanisms of seismically-induced settlement of buildings with shallow foundations on liquefiable soil. J Geotech Geoenviron Eng 136(1):151–164

Elgamal A, Yang Z, Parra E, Ragheb A (2003) Modeling of cyclic mobility in saturated cohesionless soils. Int J Plast 19:883–905

Finn WDL, Lee KW, Martin GR (1977) An effective stress model for liquefaction. J Geotech Eng Div ASCE 103(GT6):513–533

Karamitros D, Bouckovalas G, Chaloulos Y (2013) Insight into the seismic liquefaction performance of shallow foundations. J Geotech Geoenviron Eng 139(4):599–607

Karimi Z, Dashti S (2016) Numerical and centrifuge modeling of seismic soil-foundation–structure interaction on liquefiable ground. J Geo-tech Geo-environ Eng ASCE 142(1):04015061

Katona MG, Zienkiewicz OC (1985) A unified set of single step algorithms part 3: the Beta-m method, a generalization of the Newmark scheme. Int J Numer Methods Eng 21(7):1345–1359

Kramer SL, Seed BH (1988) Initiation of static liquefaction under static loading conditions. J Geotech Eng Div ASCE 114(4):412–430

Kumari S, Sawant VA, Sahoo PP (2016) Assessment of effect of cyclic frequency and soil modulus on liquefaction using coupled FEA. Indian Geotech J 46(2):124–140

Liu L, Dobry R (1997) Seismic response of shallow foundation on liquefiable sand. J Geo-tech Geo-environ Eng ASCE 123(6):557–567

Liyanapathirana DS, Poulos HG (2002) Numerical simulation of soil liquefaction due to earthquake loading. Soil Dyn Earthq Eng 22:511–523

Mehrzad B, Haddad A, Jafarian Y (2016) Centrifuge and numerical models to investigate liquefaction-induced response of shallow foundations with different contact pressures. Int J Civ Eng. https://doi.org/10.1007/s40999-016-0014-5

Mesgouez A, Lefeuve-Mesgouez G, Chambarel A (2005) Transient mechanical wave propagation in semi-infinite porous media using a finite element approach. Soil Dyn Earthq Eng 25:421–430

Nasser NS, Shokooh A (1979) A unified approach to densification and liquefaction of cohesionless sand in cyclic shearing. Can Geotech J 16(4):659–678

Oka F, Yashima A, Shibata T, Kato M, Uzuoka R (1994) FEMFDM coupled liquefaction analysis of a porous soil using an elastoplastic model. Appl Sci Res 52:209–245

Pastor M, Zienkiewicz OC (1986) A generalized plasticity hierarchical model for sand under monotonic and cyclic loading. In: Proceedings of the 2nd international symposium on numerical models in geomechanics, vol 5, no 1, pp. 141–150

Pastor M, Zienkiewicz OC, Chan AHC (1990) Generalized plasticity and the modeling of soil behaviour. Int J Numer Anal Meth Geomech 14(3):151–190

Patil VA, Sawant VA, Kousik D (2013) 2-D finite element analysis of rigid pavement considering dynamic vehicle–pavement interaction effects. Appl Math Model 37(3):1282–1294

Prevost JH (1989) DYNA1D, a computer program for nonlinear seismic site response analysis: technical documentation. Technical Report NCEER-89–0025. National Center for Earthquake Engineering Research, State University of New York at Buffalo

Seed HB (1979) Soil liquefaction and cyclic mobility evaluation for level ground during earthquakes. J Geotech Eng Div ASCE 105(GT2):201–255

Seed HB, Idriss IM (1971) Simplified procedure for evaluating soil liquefaction potential. J Soil Mech Found Div ASCE 92(SM6):249–1273

Seed HB, Lee KL (1966) Liquefaction of saturated sands during cyclic loading. J Geotech Eng ASCE 92(SM6):105–134

Seed HB, Tokimatsu H, Chung R (1985) Influence of SPT procedures in soil liquefaction resistance evaluations. J Geotech Eng ASCE 111(12):1425–1445

Simon BR, Wu JSS, Zienkiewicz OC, Paul DK (1986) Evaluation of u–w and u–p finite element methods for the dynamic response of saturated porous media using one-dimensional models. J Numer Anal Method Geomech 10:461–482

Taiebat M, Shahir H, Pak A (2007) Study of pore pressure variation during liquefaction using two constitutive models for sand. Soil Dyn Earthq Eng 27:60–72

Zienkiewicz OC, Chan AHC, Pastor M, Schrefler BA, Shiomi T (1999) Computational geomechanics with special reference to earthquake engineering. Wiley, New York